On the Identification and Modelling of Friction in a Randomly Excited Energy Harvester

P.L.Green, K.Worden, N.D.Sims

Department of Mechanical Engineering, University of Sheffield, Mappin Street, Sheffield, United Kingdom, S1 3JD

Abstract

A recent trend in energy harvesting research has been to investigate the potential benefits of deliberately introducing nonlinearities into devices to improve their performance. This has been accompanied by work dedicated to the investigation of how energy harvesters respond to excitations of a stochastic nature. The present article is concerned with those nonlinearities which are unavoidable - specifically friction. To this end, an electromagnetic energy harvester whose performance is known to be affected by friction is investigated. Initially, the governing equations of the device are derived and a differential evolution algorithm is used alongside experimental data to identify the parameter values needed to accurately model the device. This process is repeated several times using three different friction models: Coulomb, hyperbolic tangent and LuGre. For the majority of the tests conducted it was found that the Coulomb damping model was able to produce the closest match to the experimental data although the LuGre model proved more suitable in one case where a relatively high level of friction was present. Using the Coulomb damping model, the response of the device to a broadband white noise excitation is then analysed analytically using the method of equivalent linearisation, thus providing expressions which can be used to show the effect of friction on device performance. Validating these results with time domain simulations it is shown that the effects of the Duffing-type and Coulomb nonlinearities do not interact, thus allowing one to utilise the benefits of Duffing-type nonlinearities in friction-affected energy harvesting devices.

Email address: p.l.green@sheffield.ac.uk (P.L.Green)

1. Introduction

When the concept of harvesting electrical energy from ambient vibrations first became a popular research topic, a large body of work was developed which focused on the response of SDOF linear devices to sinusoidal excitations ([1, 2, 3, 4, 5] for example). Irrespective of the electromechanical coupling used (such devices typically use an electromagnetic or piezoelectric coupling) these devices were modelled with viscous dampers to simulate a combination of parasitic losses as well as the transfer of mechanical energy into the electrical domain. With regards to the devices themselves, it was found that they would only produce a useful amount of power if they were excited at resonance, thus giving them a narrow bandwidth of frequencies over which effective performance could be obtained. Additionally, it was realised that a sinusoidal excitation was a poor representation of ambient vibrations: these are usually non-periodic, have time dependent dominant frequencies and often have to be viewed as being stochastic in nature.

The narrow operational bandwidth of SDOF energy harvesters led to several investigations into devices which could tune their natural frequency so that they could adapt to changes in the dominant frequency of excitation [6, 7, 8, 9]. As well as this, the concept of deliberately introducing Duffing-type nonlinearities into such devices to enhance performance has been widely investigated. This led to a large variety of nonlinear energy harvesters which, broadly speaking, can be separated into two varieties: monostable [10, 11, 12, 13, 14] and bistable [15, 16, 17] (depending on the number of potential equilibrium points they possess). The applicability of these solutions to the harvesting of energy from some real ambient excitations was examined in [18]. An interesting study was conducted by McInnes et al [19] in which a stochastically excited bistable energy harvester was described which, through oscillating the height of the potential energy barrier, was able to use the phenomenon of stochastic resonance to improve power output. While much work has been focused on energy harvesters with Duffing-type nonlinearities it is worth noting that this is not the only form of nonlinearity which has been investigated - reference [20] details a monostable device whose bandwidth was improved via the use of stopper-type nonlinearities for example.

The present work focuses on the monostable device proposed by Mann and Sims [10] who developed an electromagnetic energy harvester which used the restoring force between two magnets of opposing poles to create a system with nonlinearities similar to that of the monostable Duffing oscillator. The device was constructed in the hope that the nonlineaity

would improve its useful bandwidth. The response of this energy harvester to Gaussian white noise excitations was then analysed analytically using the Fokker-Planck-Kolmogorov (FPK) equation in several works [21, 22]. Using closed-form solutions it was shown that, when subject to a Gaussian white noise excitation, the nonlinear term had no effect on power output [21] but could be used to reduce device rattle space without harming performance [22].

During an experimental investigation of such a device (as part of [22] and [23]) it was observed that the response of the energy harvester was sensitive to the effects of friction. For this reason, it was thought important to investigate the effect of this unavoidable nonlinearity on the response of the device to random excitations. Consequently, the aim of this paper is to analyse a variety of friction models in an attempt to develop a numerical simulation which is able to mimic the response of a real device as effectively as possible. To this end, using numerical simulations alongside experimental data, a self-adaptive differential evolution (SADE) algorithm [24, 25] is used to analyse the suitability of three different friction models (Coulomb, hyperbolic tangent and LuGre). Having identified a suitable model, it is then shown that the technique of equivalent linearisation can be used to accurately model the effects of friction on the power output of the device when excited by Gaussian white noise. Finally, by comparing results using equivalent linearisation with digital simulations it is shown that there is no significant interaction between the Duffing-type and Coulomb nonlinearities.

2. Energy harvester

As mentioned previously the main focus of this paper is the device proposed by Mann and Sims [10] (Figure 1). This device consists of two 'outer magnets' which are attached to the shell of the device and are orientated such that their poles repel those of a 'centre magnet'. The centre magnet is free to oscillate such that, as a consequence of the magnetic fields acting on it from the outer magnets, a nonlinear restoring force similar to the hardening spring Duffing oscillator is created. When subjected to a base excitation (y in Figure 1), the centre magnet will oscillate relative to the outer shell of the device thus creating an electric current in coils wound around the device (by Faraday's law).

2.1. Governing equations

A lumped parameter model of the device in question is shown in Figure 2 (a). Throughout this work it is assumed that the device is delivering electrical energy to a load resistance.

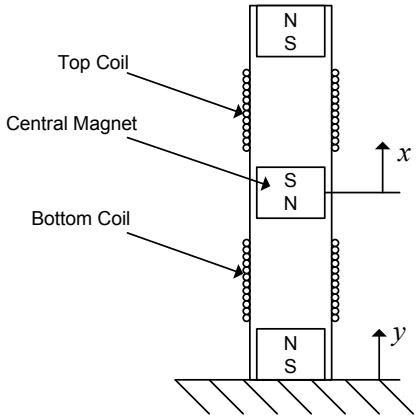

Figure 1: Schematic diagram of device proposed by Mann and Sims [10].

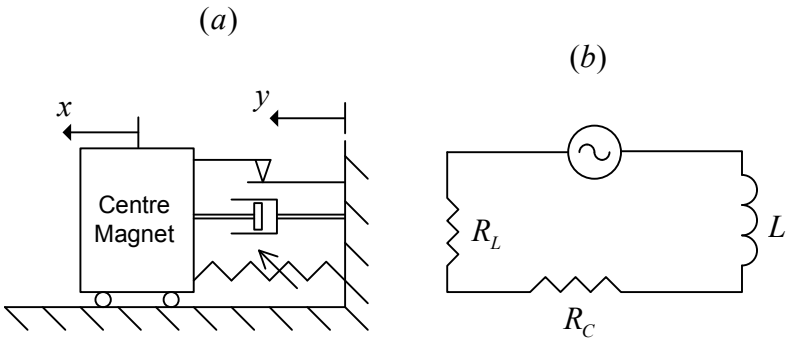

Figure 2: Schematics of (a) mechanical and (b) electrical elements of the device.

The resulting circuitry for the device is shown in Figure 2 (b) where L is the inductance that arises as a result of the electromagnetic coupling and R_L and R_C are the load and coil resistances respectively.

To a good approximation, the equation of motion of this device is:

$$m\ddot{z} + (c_e + c_m)\dot{z} + kz + k_3 z^3 + F = -m\ddot{y} \tag{1}$$

where z is the relative displacement between the shaker base and centre magnet:

$$z = (x - y), \tag{2}$$

m is the mass of the centre magnet, c_e and c_m are damping due to electrical and mechanical effects, k and k_3 are linear and nonlinear stiffness terms, F is the force due to friction and $\ddot{y}$ represents the base acceleration. It is worth noting that if one assumes negligible inductance and a linear flux displacement relationship ($d\Phi/dz = \alpha$, where α is constant) then the damping due to the electromagnetic coupling is given by:

$$c_e = \alpha^2 \frac{1}{R_L + R_C}. \tag{3}$$

For the interested reader this relationship is derived and experimentally validated in [22]. Throughout this work the response of the device was simulated in Matlab's Simulink environment.

2.2. Friction models

The force on the centre magnet as a result of friction (F) was represented using three different friction models: Coulomb, hyperbolic tangent and LuGre [26]. The properties of each model are briefly discussed in the following sections.

2.2.1. Coulomb

This is among the earliest and best known friction models. Using the Coulomb damping model the restoring force due to friction is given by:

$$F = F_c \operatorname{sgn}(\dot{z}) \tag{4}$$

where F_c is a parameter to be identified and sgn represents the signum function:

$$\operatorname{sgn}(\dot{z}) = \begin{cases} 1, & \dot{z} > 0 \\ 0, & \dot{z} = 0 \\ -1, & \dot{z} < 0 \end{cases} \tag{5}$$

With one parameter, the obvious advantage of the Coulomb damping model is its simplicity although it is unable to model some of the phenomena which are typically associated with friction-affected systems (this is discussed more with regards to the LuGre model). Additionally, the discontinuity of the signum function at zero can make analytical progress difficult.

2.2.2. Hyperbolic tangent

The second model that will be investigated is the hyperbolic tangent friction model:

$$F = F_c \tanh(\beta \dot{z}). \tag{6}$$

This has the property that, while requiring an extra parameter (β in this case), the model is able to approximate the Coulomb damping model without being discontinuous. This is because it reduces to the signum function as β approaches infinity:

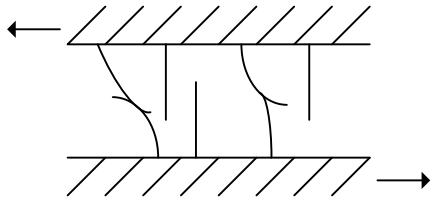

Figure 3: In the LuGre model friction is represented by the interaction of randomly distributed elastic bristles.

$$\lim_{\beta \to \infty} \tanh(\beta \dot{z}) = \mathrm{sgn}(\dot{z}). \tag{7}$$

2.2.3. LuGre

The LuGre model [26] is based on the assumption that the interaction between two surfaces can be modelled as that of rigid bodies which make contact via a set of randomly distributed 'bristles' (see Figure 3).

The average displacement of the bristles is modelled using:

$$\dot{\Theta} = \dot{z} - \frac{|\dot{z}|}{g(\dot{z})}\Theta \tag{8}$$

where Θ is the average bristle displacement and $g(\dot{z})$ is a function which is chosen depending on the material properties of the system. Equation (8) is in state-space form (in other words, $\dot{\Theta}$ is expressed as a function of Θ) thus allowing it to be evaluated using the same numerical integration techniques that are used to simulate the response of the energy harvester. The friction force exerted on the mass is given by:

$$F = \sigma_0 \Theta + \sigma_1 \dot{\Theta} \tag{9}$$

where σ_0 and σ_1 are parameters to be found. The LuGre model belongs to the Duhem class of hysteretic models [27, 28]. It takes account of the Stribeck effect (the phenomenon that, at low velocities, friction force decreases with increasing velocity) and had been used to accurately replicate the response of an experimental system with hysteretic dynamics [29]. To account for the Stribeck effect the function $g(\dot{z})$ will be defined as:

$$\sigma_0 g(\dot{z}) = F_c + (F_s - F_c)e^{-(\dot{z}/\dot{z}_s)^2} \tag{10}$$

where F_s represents stiction force, F_c is the Coulomb friction level and $\dot{z}_s$ is the Stribeck velocity (the point at which the steady-state friction force begins to dip as velocity increases)

[28]. While this model requires the identification of five parameters (σ_0, σ_1, F_c, F_s and $\dot{z}_s$) it accounts for the majority of phenomenon associated with friction (friction lag, spring-like behavior in stiction and varying break-away force).

3. Experiment

The mechanical properties of the system were identified using the apparatus shown in Figure 4. The device was attached to an electromagnetic shaker using an aluminium extension piece while the centre magnet was allowed to run along an aluminium rod via two sets of linear bearings. A linear variable differential transducer (LVDT) was used to measure the displacement of the shaker table. This signal was then fed through a proportional integral differential (PID) controller to allow control of the shaker table displacement.

Using the controller, the shaker was excited with a displacement signal that resulted in a white noise acceleration with a flat power spectral density between 4 and 20 Hz. As the device had a natural frequency of approximately 8 Hz, it was thought that the bandwidth of the acceleration spectrum was sufficiently large to excite the relevant dynamics of the system. During each test the displacement of the centre magnet was recorded using the laser (also shown in Figure 4).

Using the shaker table time histories allowed any model of the device to be excited with the same displacement time history that had been used experimentally. Comparing the model and experiment centre magnet time histories formed an essential part of the parameter identification scheme used. This is discussed in the next section.

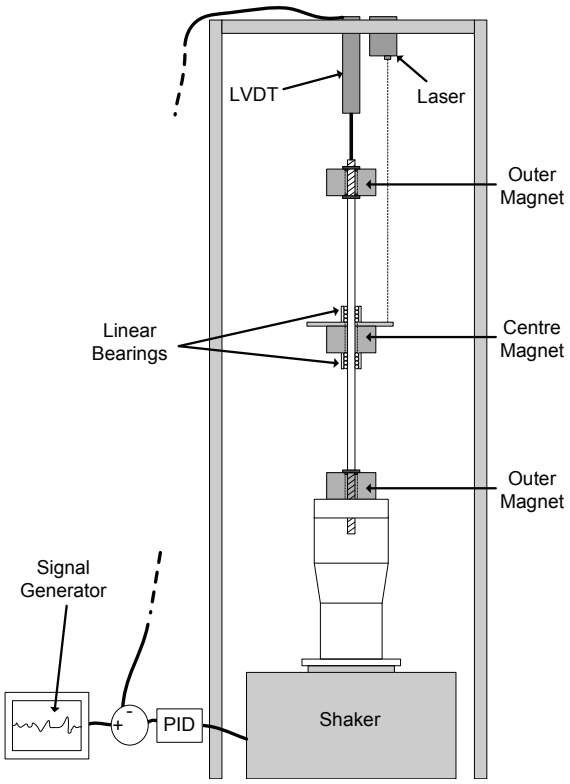

Figure 4: Schematic of experimental apparatus used to validate the mechanical parameters of the device.

3.1. Parameter Identification

Having measured the mass of the centre magnet the other model parameters were identified using a self-adaptive differential evolution (SADE) algorithm [24, 25]. Having excited the model with the same base displacement signal as was used experimentally, a cost function was used to describe the level of similarity between the time response of the model compared with that of the experiment. Throughout this work the cost function is defined as:

$$J(\boldsymbol{\theta}) = \frac{100}{N\sigma_z^2}\sum_{i=1}^{N}(z_i - \hat{z}_i(\boldsymbol{\theta}))^2 \tag{11}$$

where $\boldsymbol{\theta}$ is the vector of unknown parameters, i represents the point in the time history vector, z_i and σ_z^2 represent the time history and variance of the experimentally obtained relative displacement and $\hat{z}_i$ represents the relative displacement according to the simulation. The cost function is normalised such that if the model simply produced the mean of the experimental result (denoted $\bar{z}$) then the function will return a value of 100:

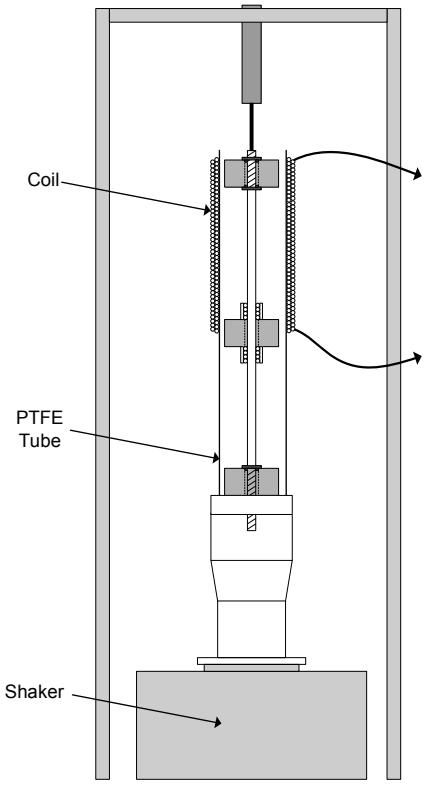

Figure 5: Schematic of experimental apparatus used to validate the electrical parameters of the device.

$$J(\boldsymbol{\theta}) = \frac{100}{N\sigma_y^z} \sum_{i=1}^{N} (z_i - \bar{z})^2 = 100 \tag{12}$$

It is shown in [25] that a cost function of less than five represents a reasonably good correlation, and that less than one can be considered excellent. The aim at this stage then, was to use SADE to identify the model parameters which minimised J (equation (11)) for each of the friction models being investigated.

Once the mechanical parameters of the device were identified, 83 turns of 0.5 mm diameter copper coil were wrapped around a PTFE tube which was subsequently attached to the shaker base (as shown in Figure 5). The output from the coil was then fed through a load resistor. The resistance of the coil was found to be 0.48 Ohms and the inductance was found to be negligible.

The relationship between the magnetic flux and the relative displacement of the centre magnet for a single turn of coil was found using the finite element package FEMM. Following an assumption made in the previous section, a linear approximation of the flux-displacement relationship was made. Figure 6 shows that the approximation was chosen under the as-

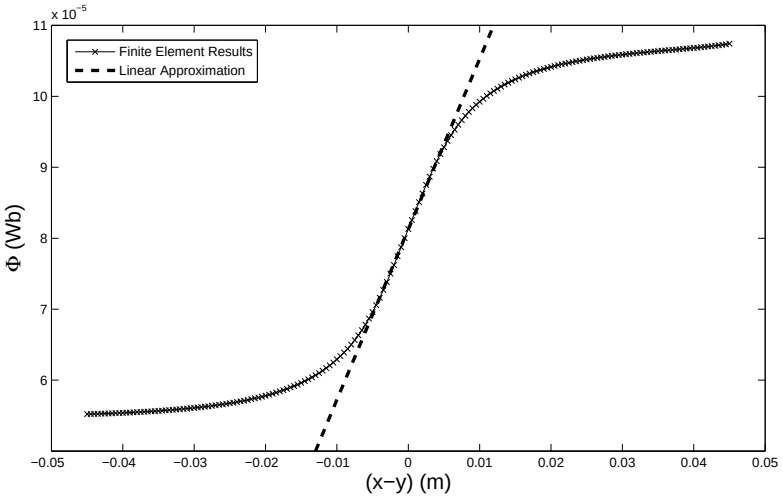

Figure 6: Finite Element simulation of flux displacement relationship. Dashed and solid lines represent simulation results and the linear approximation respectively.

sumption that only relatively small centre magnet displacements would take place. From finite element simulations it was found that $\alpha_1 = 0.0024$ Wb/m (where α_1 represents the flux displacement relationship for one turn of coil). Multiplying by the number of turns on the device it was found that $\alpha = 0.1992$ Wb/m. This procedure was also used in [22].

4. Results

In this section the results of the parameter identification investigation are detailed. Firstly, the ability of the different friction models to replicate the mechanics of the device are analysed. In the subsequent section, having identified the most suitable friction model, the ability of the simulations to replicate the voltage output of the experimental device when delivering power to a load resistor is analysed.

Nine different experiments were conducted - each using a different intensity of band-limited white noise. The root-mean-square (RMS) value of each excitation signal is shown in Table 1. Initially, test number 3 was used as the training data for SADE (shown as 'training data 1' in Table 1). The parameter values identified are shown in Table 2 (training data 1). The identified parameter values were then used to compare the model response with that of the experiment for all the other test conditions. Again, the ability of the model to replicate the response of the experiment was quantified using the cost function (equation (11)).

	Test number	RMS($\ddot{y}$) (m/s^2)
	1	1.07
	2	1.21
Training data 1:	3	1.34
	4	1.54
	5	1.67
	6	1.84
	7	1.96
Training data 2:	8	2.12
	9	2.22

Table 1: RMS base acceleration for each excitation condition.

Model	Parameter	Value (training data 1)	Value (training data 2)	Units
No Friction	c	0.116	0.079	Ns/m
	k	54.8	54.2	N/m
	k_3	112620	119210	N/m^3
Coulomb	c	0.049	0.047	Ns/m
	k	57.4	56.1	N/m
	k_3	70742	91894	N/m^3
	F_c	0.0058	0.0065	N
Hyperbolic	c	0.049	0.047	Ns/m
tangent	k	57.5	56.1	N/m
	k_3	68956	91798	N/m^3
	F_c	0.0058	0.0065	N
	β	4.8×10^8	8.3×10^8	s/m
LuGre	c	0.055	0.051	Ns/m
	k	59.7	58.1	N/m
	k_3	64926	79788	N/m ^{3}
	σ_0	1.98	4.9	N/m
	σ_1	0.18	0.19	Ns/m
	F_c	0.0008	0.0007	N
	F_s	0.008	0.0006	N
	$\dot{z}_s$	0.007	0.0006	m/s

Table 2: Identified Parameters for each friction model using test 3 and test 8 as training data.

Figure 7 (a) compares the performance of each friction model using the parameters identified when test 3 was used as training data. It is immediately obvious that the inclusion of a friction model has greatly improved the ability of the simulations to replicate the response of the experiment. It can also be seen that very similar cost values are realised for the Coulomb and hyperbolic tangent models over the entire range of tests. Recalling the governing equations of both models:

$$F = F_c \operatorname{sgn}(\dot{z}) \tag{13}$$

$$F = F_c \tanh(\beta \dot{z}) \tag{14}$$

after consulting the identified parameters in Table 2 (training data 1), it is clear that these two models will behave in a similar manner. This is because the same value of F_c was identified in each case and, as a result of a high value for β, the hyperbolic tangent model is forming a close approximation to the signum function used in the Coulomb damping model. Perhaps one of the most interesting results from this investigation is that the Coulomb and hyperbolic tangent models have consistently outperformed the LuGre model for all of the test conditions except for test 8. This also happens to be the test case where friction seemed to be having the largest effect on device response (as this is where the simulations without a friction model performed the worst).

Indeed, the test that was used as training data (test 3) also happens to be the test where friction appeared to be the least significant. This raises the possibility that the dynamics of the system were not sufficiently friction-affected to allow proper identification of the parameters in the LuGre model. For this reason the identification process was repeated using the most friction affected test (test 8) as the training data (shown as 'training data 2' in Table 1). The resulting parameters are shown in Table 2 (training data 2).

Using this new training data it was found that, as before, the hyperbolic tangent model formed a close approximation to the Coulomb damping model. For both models a higher value of F_c was identified when test 8 was used as training data - this confirms the hypothesis that friction affected this test more than test 3. It is also interesting to note that the LuGre model now outperforms the Coulomb and hyperbolic tangent models in more cases than in the previous case. This confirms that the use of a more friction-affected test as training data has led to better parameter estimates for the LuGre model.

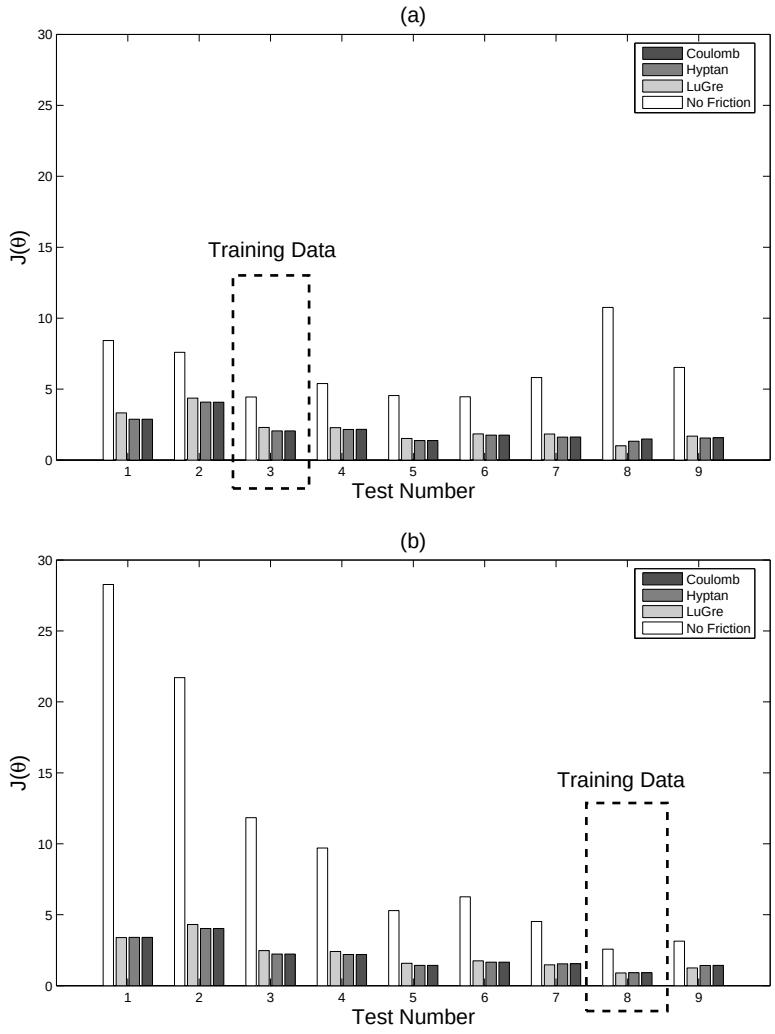

Figure 7: Cost between experiment and simulation time histories for different tests having used (a) test 3 and (b) test 8 as training data.

Figure 7 (b) compares the performance of each friction model using the parameters identified when test 8 was the training data. While the use of a different test as training data has improved the performance of the viscous model in some cases it has also dramatically impaired it in others. This confirms that such a model is poorly suited to model the dynamics of the device over its full range of operating conditions.

Finally, it is worth noting that the device investigated here is relatively large for an energy harvester - in fact the recent increase in energy harvesting research is often thought to be as a result of advances in MEMS technology allowing the construction of devices on the micro-scale. Such devices may be much more susceptible to the effects of friction. For this device though (which has a height of roughly 30cm), it is clear that the Coulomb damping

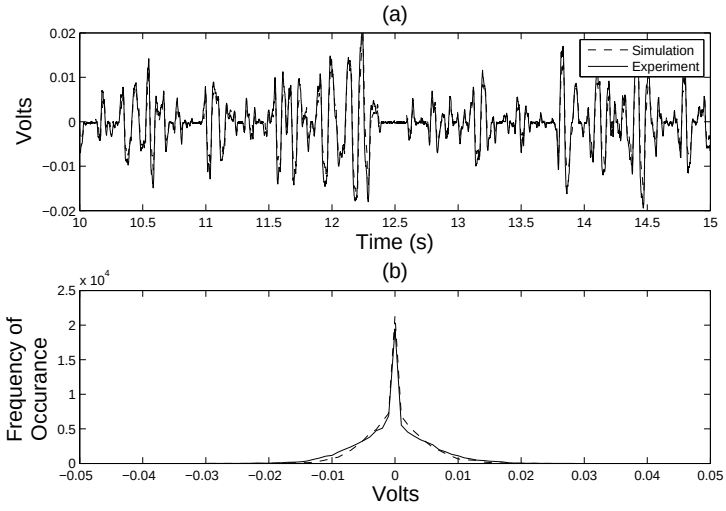

Figure 8: Comparison of simulation (dashed line) and experimental (solid line) (a) time history and (b) histogram for test condition 6.

model is usually sufficiently accurate.

Having decided to include the Coulomb damping model, the ability of the simulations to predict the voltage output of the device was analysed. Figure 8 shows an excellent agreement between the simulation and experiment. With regards to the histogram (Figure 8 (b)) it is interesting to note a large 'spike' at zero volts. This is a result of friction preventing the centre magnet from moving relative to the device outer casing thus resulting in a voltage output close to zero. Indeed, if one neglects to use a friction model, this spike disappears from the simulated histograms.

5. Equivalent linearisation

5.1. Application to Coulomb damping

As mentioned in the introduction to this work, the stochastic nature of ambient vibrations has led to many authors focusing on the response of energy harvesters to random excitations - often Gaussian white noise. It has been shown that the response of a monostable energy harvesting device with Duffing-type nonlinearities to the afore mentioned excitation conditions can be analysed using a closed form solution of the corresponding FPK equation [21, 22]. However, the inclusion of Coulomb damping makes the FPK equation for this system difficult to solve. Consequently, in this section, the technique of equivalent linearisation will be used in conjunction with known solutions from the FPK equation to model the effects of friction on a randomly excited device.

Equivalent linearisation involves finding a linear system which can replicate the response of its nonlinear counterpart as closely as possible. With regards to energy harvesting, the aim of this section is create an equivalent linear system which allows one to approximate the effect of friction on the power output of the device to a sufficient degree of accuracy. Findings from previous works [21, 22] have established that, when excited by Gaussian white noise, the nonlinear spring term k_3 has no effect on power output and can therefore be neglected in the following analysis. However, these studies did not include friction. In the present study it is assumed that the nonlinear stiffness still has no effect on power output even when friction is present. We then test this assumption using simulated data. To that end, a SDOF system with linear spring term and velocity dependent nonlinearity is considered:

$$m\ddot{z} + f(\dot{z}) + kz = mw(t) \tag{15}$$

where $w(t)$ is a Gaussian white noise excitation with:

$$E[w(t)] = 0 \tag{16}$$

and

$$E[w(t_1)w(t_2)] = \frac{S}{2}\delta(t_2 - t_1) \tag{17}$$

where E represents the expected value, S the height of the noise power spectral density and δ is the Dirac delta function. The aim of equivalent linearisation is to find a linear system of the form:

$$m\ddot{z} + c_{eq}\dot{z} + kz = mw(t) \tag{18}$$

where c_{eq} is chosen such that the linear response is able to match the response of the nonlinear system as closely as possible (as quantified using a least-squares measure). In [30] it is shown that, for the case of Coulomb damping, the equivalent damping term in equation (18) is given by the following integral:

$$c_{eq} = c + \frac{F_c}{\sqrt{2\pi}\sigma_{\dot{z}eq}^3}\int_{-\infty}^{\infty} \exp\left(-\frac{\dot{z}^2}{2\sigma_{\dot{z}eq}^2}\right)\dot{z}\,\mathrm{sgn}(\dot{z})d\dot{z} \tag{19}$$

(as $E[\dot{z}] = 0$) where $\sigma_{\dot{z}eq}^2$ is the variance of the linear equivalent system's velocity probability density function which, from [31], is known to be:

$$\sigma_{\dot{z}eq}^2 = \frac{Sm}{4c_{eq}}. \tag{20}$$

By writing:

$$\mathrm{sgn}(\dot{z}) = \frac{|\dot{z}|}{\dot{z}} \tag{21}$$

one obtains:

$$\begin{aligned} c_{eq} &= c + \frac{F_c}{\sqrt{2\pi}\sigma_{\dot{z}eq}^3} \int_{-\infty}^{\infty} \exp\left(-\frac{\dot{z}^2}{2\sigma_{\dot{z}eq}^2}\right) |\dot{z}| d\dot{z} \\ &= c + \frac{F_c}{\sqrt{2\pi}\sigma_{\dot{z}eq}^3} 2 \int_{0}^{\infty} \exp\left(-\frac{\dot{z}^2}{2\sigma_{\dot{z}eq}^2}\right) \dot{z} d\dot{z}. \end{aligned} \tag{22}$$

Recalling that,

$$\frac{d}{d\dot{z}}\left(\exp\left(-\frac{\dot{z}^2}{2\sigma_{\dot{z}eq}^2}\right)\right) = -\frac{\dot{z}}{\sigma_{\dot{z}eq}^2} \exp\left(-\frac{\dot{z}^2}{2\sigma_{\dot{z}eq}^2}\right) \tag{23}$$

then,

$$-\sigma_{\dot{z}eq}^2 \exp\left(-\frac{\dot{z}^2}{2\sigma_{\dot{z}eq}^2}\right) = \int \exp\left(-\frac{\dot{z}^2}{2\sigma_{\dot{z}eq}^2}\right) \dot{z} d\dot{z}. \tag{24}$$

Substituting this result into equation (22) yields:

$$c_{eq} = c + \frac{F_c}{\sqrt{2\pi}\sigma_{\dot{z}eq}^3}(-2\sigma_{\dot{z}eq}^2)\left[\exp\left(-\frac{\dot{z}^2}{2\sigma_{\dot{z}eq}}\right)\right]_0^{\infty} \tag{25}$$

therefore:

$$c_{eq} = c + \frac{2F_c}{\sqrt{2\pi}\sigma_{\dot{z}eq}}. \tag{26}$$

Using the equivalent linear velocity variance (equation (20)) this may be written:

$$c_{eq} = c + \frac{4F_c}{\sqrt{2\pi}}\sqrt{\frac{c_{eq}}{Sm}}, \tag{27}$$

therefore:

$$(c_{eq} - c)^2 = \left(\frac{4F_c}{\sqrt{2\pi}}\right)^2 \frac{c_{eq}}{Sm}, \tag{28}$$

which, after a little manipulation, can be written:

$$c_{eq}^2 + c_{eq}\left[-2c - \frac{8F_c^2}{\pi Sm}\right] + c^2 = 0. \tag{29}$$

After solving with the quadratic formula and neglecting negative values of damping as being unphysical, the equivalent damping term is given by:

$$c_{eq} = c + \frac{4F_c^2}{\pi Sm} + \frac{1}{2}\sqrt{\left(-2c - \frac{8F_c^2}{\pi Sm}\right)^2 - 4c^2}. \tag{30}$$

The expected power delivered to the electrical domain is given by:

$$E[P_e] = E[c_e \dot{z}^2] = c_e E[\dot{z}^2] \tag{31}$$

which, as $E[\dot{z}] = 0$, can be written:

$$E[P_e] = c_e \sigma_{\dot{z}}^2 = c_e \frac{Sm}{4c_{eq}} \tag{32}$$

where c_{eq} is given by equation (30). Figure 9 shows a comparison between the equivalent linearisation approach and the results of numerical simulations of equation (1) for 3 different values of power spectral density height (S) for the cases where (a) $k_3 = 0$ and (b) $k_3 = 500000$ N/m^3. In all of the cases shown it is clear that the equivalent linearisation approach has accurately modelled the effect of friction on power delivered to the electrical domain. What is perhaps most interesting about this result is that the ability of the equivalent linear system to replicate the response of the digital simulation does not appear to be affected by the presence of the Duffing-type nonlinearity (k_3). With regards to energy harvester design this is a useful result as it demonstrates that the intentionally introduced Duffing-type nonlinearity is not interacting with the unavoidable friction nonlinearity in a way which can be detrimental to the device performance. Consequently, it can be concluded that the benefits one can achieve via the addition of the hardening-spring nonlinearity with regards to rattle space (see [22]) are still possible despite the presence of friction.

6. Discussion and future work

This paper is concerned with the effects of friction losses on the response of an energy harvesting device. It is clear that friction will be present in the device detailed in this work (as linear bearings are used to prevent the centre magnet from experiencing sideways / rotational motion). If one considers devices of the cantilevered beam type it is interesting to note that, although friction will not be effecting such a device, some recent works have begun to focus on the different types of energy loss mechanisms that are present in such systems. For example, the work detailed in [32] was concerned with the simulation of piezoelectric beam type devices with a model where material damping dominated the response (as apposed to air damping).

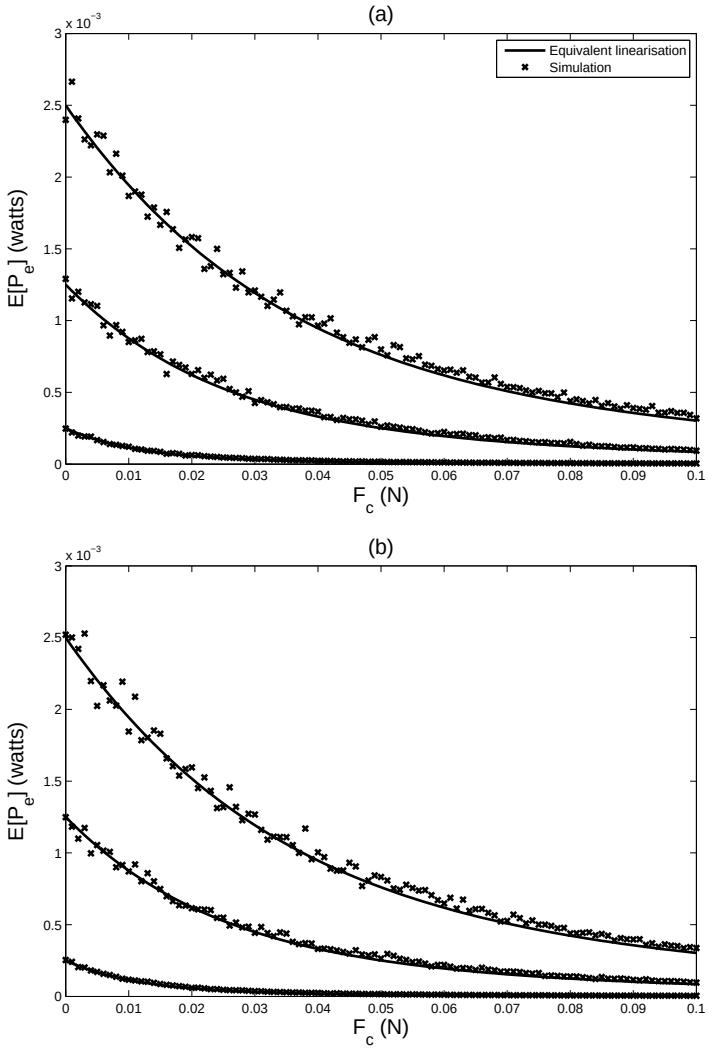

Figure 9: The effect of Coulomb damping on expected power output where $c_m = c_e = 0.1$ Ns/m and, from top to bottom, $S = 1$, 0.5 and 0.1 (m/s^2)/Hz respectively. Figures (a) and (b) represent cases where $k_3 = 0$ and 500000 N/m^3 respectively while all other parameters are the same as those shown in Table 2 (Coulomb model). Crosses and solid line represent results according to simulation and equivalent linearisation respectively.

In the previous section it was shown that the technique of equivalent linearisation could be used to accurately predict the effect of Coulomb damping on the response of the device. While its application in this case was successful it should be noted that, by using an equivalent linear system, this method cannot be used to replicate some of the phenomena associated with nonlinear systems (super-harmonics for example). The effect to these higher harmonics will depend on the level of nonlinearity and nature of excitation - future work could be directed towards finding closed-form or approximate solutions to the stationary FPK equation of a SDOF system with Coulomb damping such that these effects can be analysed.

7. Conclusions

In this work, the effect of friction on the response of an electromagnetic energy harvester with Duffing-type nonlinearities was analysed. Performing system identification using a differential evolution algorithm in conjunction with experimental tests, it was shown that considering the effects of friction is essential if one is to accurately model the response of this type of energy harvester. Following the analysis of several different friction models, it was found that the use of the Coulomb damping model led to the best match between experiment and simulation. The technique of equivalent linearisation was then used to develop an analytical expression which could accurately predict the effects of Coulomb damping on the power output of a randomly excited energy harvesting device. Comparing the response of time domain simulations with the results anticipated using the equivalent linearisation approach it was shown that, when under a Gaussian white noise excitation, there appears to be no interaction between the Duffing-type and the Coulomb nonlinearities thus allowing exploitation of Duffing-type nonlinearities in friction-affected devices.

[1] C.B. Williams and R.B. Yates. Analysis of a micro-electric generator for microsystems. *Sensors and Actuators A: Physical*, 52(1-3):8 – 11, 1996.

[2] P.D. Mitcheson, T.C. Green, E.M. Yeatman, and A.S. Holmes. Architectures for vibration-driven micropower generators. *Journal of Microelectromechanical Systems*, 13(3):429–440, JUN 2004.

[3] N.G. Stephen. On energy harvesting from ambient vibration. *Journal of Sound and Vibration*, 293(1-2):409 – 425, 2006.

[4] B.P. Mann and N.D. Sims. On the performance and resonant frequency of electromagnetic induction energy harvesters. *Journal of Sound and Vibration*, 329(9):1348–1361, APR 26 2010.

[5] S.P. Beeby, M.J. Tudor, and N.M. White. Energy harvesting vibration sources for microsystems applications. *Measurement Science and Technology*, 17(12):R175, 2006.

[6] V.R. Challa, M.G. Prasad, Y. Shi, and F.T. Fisher. A vibration energy harvesting device with bidirectional resonance frequency tunability. *Smart Materials and Structures*, 17(1), 2008.

[7] W. Al-Ashtari, M. Hunstig, T. Hemsel, and W. Sextro. Frequency tuning of piezoelectric energy harvesters by magnetic force. *Smart Materials and Structures*, 21(3), 2012.

[8] R. Masana and M.F. Daqaq. Electromechanical modeling and nonlinear analysis of axially loaded energy harvesters. *Journal of Vibration and Acoustics, Transactions of the ASME*, 133(1), 2011.

[9] Y.-J. Wang, C.-D. Chen, C.-K. Sung, and C. Li. Natural frequency self-tuning energy harvester using a circular halbach array magnetic disk. *Journal of Intelligent Material Systems and Structures*, 23(8):933–943, 2012.

[10] B.P. Mann and N.D. Sims. Energy harvesting from the nonlinear oscillations of magnetic levitation. *Journal of Sound and Vibration*, 319(1-2):515–530, JAN 9 2009.

[11] S.C. Stanton, C.C. McGehee, and B.P. Mann. Reversible hysteresis for broadband magnetopiezoelastic energy harvesting. *Applied Physics Letters*, 95(17), 2009.

[12] D.A.W. Barton, S.G. Burrow, and L.R. Clare. Energy harvesting from vibrations with a nonlinear oscillator. *Journal of Vibration and Acoustics, Transactions of the ASME*, 132(2):0210091–0210097, 2010.

[13] D.D. Quinn, A.L. Triplett, L.A. Bergman, and A.F. Vakakis. Comparing linear and essentially nonlinear vibration-based energy harvesting. *Journal of Vibration and Acoustics, Transactions of the ASME*, 133(1), 2011.

[14] B. Marinkovic and H. Koser. Demonstration of wide bandwidth energy harvesting from vibrations. *Smart Materials and Structures*, 21(6), 2012.

[15] A. Erturk and D.J. Inman. Broadband piezoelectric power generation on high-energy orbits of the bistable duffing oscillator with electromechanical coupling. *Journal of Sound and Vibration*, 330(10):2339–2353, 2011.

[16] B.P. Mann and B.A. Owens. Investigations of a nonlinear energy harvester with a bistable potential well. *Journal of Sound and Vibration*, 329(9):1215–1226, 2010.

[17] D.N. Betts, H.A. Kim, C.R. Bowen, and D.J. Inman. Optimal configurations of bistable piezo-composites for energy harvesting. *Applied Physics Letters*, 100(11), 2012.

[18] P.L. Green, E. Papatheou, and N.D. Sims. Energy harvesting from human motion and bridge vibrations: An evaluation of current nonlinear energy harvesting solutions. *Journal of Intelligent Material Systems and Structures*, 2013.

[19] C.R. McInnes, D.G. Gorman, and M.P. Cartmell. Enhanced vibrational energy harvesting using nonlinear stochastic resonance. *Journal of Sound and Vibration*, 318(4-5):655–662, 2008.

[20] H. Liu, C. Lee, T. Kobayashi, C.J. Tay, and C. Quan. A new s-shaped mems pzt cantilever for energy harvesting from low frequency vibrations below 30 hz. *Microsystem Technologies*, 18(4):497–506, 2012.

[21] M.F. Daqaq. Response of uni-modal duffing-type harvesters to random forced excitations. *Journal of Sound and Vibration*, 329(18):3621–3631, AUG 30 2010.

[22] P.L. Green, K. Worden, K. Atallah, and N.D. Sims. The benefits of duffing-type nonlinearities and electrical optimisation of a mono-stable energy harvester under white gaussian excitations. *Journal of Sound and Vibration*, 2012.

[23] P.L. Green, K. Worden, K. Atallah, and N.D. Sims. The effect of duffing-type nonlinearities and coulomb damping on the response of an energy harvester to random excitations. *Journal of Intelligent Material Systems and Structures*, 0(0):0, 2012.

[24] K. Worden and G. Manson. On the identification of hysteretic systems, part i: an extended evolutionary scheme. In *Nonlinear Modeling and Applications, Volume 2*, pages 67–75. Springer, 2011.

[25] K. Worden and G. Manson. On the identification of hysteretic systems. part i: Fitness landscapes and evolutionary identification. *Mechanical Systems and Signal Processing*, 29:201–212, 2012.

[26] de Wit, C. Canudas, H. Olsson, K.J. Astrom, and P. Lischinsky. New model for control of systems with friction. *IEEE Transactions on Automatic Control*, 40(3):419–425, 1995.

[27] J. Oh and D.S. Bernstein. Semilinear duhem model for rate-independent and rate-dependent hysteresis. *Automatic Control, IEEE Transactions on*, 50(5):631–645, 2005.

[28] J. Oh, A.K. Padthe, D.S. Bernstein, D.D. Rizos, and S.D. Fassois. Duhem models for hysteresis in sliding and presliding friction. In *Decision and Control, 2005 and 2005 European Control Conference. CDC-ECC'05. 44th IEEE Conference on*, pages 8132–8137. IEEE, 2005.

[29] A.K. Padthe, J. Oh, and D.S. Bernstein. On the lugre model and friction-induced hysteresis. In *American Control Conference, 2006*, pages 6–pp. IEEE, 2006.

[30] K. Worden and G.R. Tomlinson. *Nonlinearity in structural dynamics: detection, identification, and modelling*. Institute of Physics Pub., 2001.

[31] C.W.S. To. *Nonlinear random vibration: analytical techniques and applications*. Advances in Mechanical Engineering Series. Swets & Zeitlinger Publishers, 2000.

[32] S.C. Stanton, A. Erturk, B.P. Mann, E.H. Dowell, and D.J. Inman. Nonlinear nonconservative behavior and modeling of piezoelectric energy harvesters including proof mass effects. *Journal of Intelligent Material Systems and Structures*, 23(2):183–199, 2012.